A major purpose of the Technical Information Center is to provide the broadest dissemination possible of information contained in DOE's Research and Development Reports to business, industry, the academic community, and federal, state and local governments.

Although a small portion of this report is not reproducible, it is being made available to expedite the availability of information on the research discussed herein.

LA-UR--85-4393

DE86 004745

RECEIVED BY OSTI JAN 08 1986

CONF-860391--2

TITLE UNIAXIAL STRAIN TESTING OF SOILS IN A SPLIT HOPKINSON PRESSURE BAR

AUTHOR(S) Conrad W. Felice (USAF, AFWL)
Edward S. Gaffney (ESS-5)
Joseph A. Brown (ESS-3)

SUBMITTED TO Second International Symposium on Numerical Methods
in Geomechanics
Ghent State University
Ghent, BELGIUM
31 March - 4 April 1986

MASTER

Los Alamos Los Alamos National Laboratory
Los Alamos, New Mexico 87545

FORM NO 836 R4

UNIAXIAL STRAIN TESTING OF SOILS IN A SPLIT HOPKINSON PRESSURE BAR

C. W. Felice, E. S. Gaffney*, and J. A. Brown*

Air Force Weapons Lab, Kirtland AFB, New Mexico, USA
*Los Alamos National Lab, Los Alamos, New Mexico, USA

The split-Hopkinson pressure bar (SHPB) technique has been adapted to measure the dynamic response of soil to impulse loads. The experimental technique is relatively simple and can investigate soil response in regimes beyond the capabilities of current equipment used for soil dynamic laboratory investigations. Soils have several characteristics which must be considered in designing a SHPB experiment and evaluating the data (e.g., low wave speeds, nonlinear hysteretic behavior, and low unconfined compressive strength compared to the applied loads). Insight has been gained as to how these factors affect experimental accuracy and data reliability. The ability to replicate experimental results has been established. Also, the stress-strain response was found to be governed by the initial gas porosity of the specimen. No strain-rate dependence was found at strains less than the initial gas porosity. To model the response of dry desert alluvium, a microphysical constitutive equation has been devised.

INTRODUCTION

Over the last 35 years the split-Hopkinson pressure bar (SHPB) technique has been used as a tool for investigating the response of metals, rocks, ceramics, foams, and other materials to short duration compressive impulse loads (e.g., Lindholm, 1964; Hodge and Wasley, 1969; Christensen, Swanson, and Brown, 1972). Some of the SHPB devices in use today can apply stresses in excess of 1,000 MPa with loading times on the order of 0.05 ms (Gaffney and Brown, 1984). Until recently, the SHPB technique has not been readily applied to the field of soil mechanics (Felice, 1985). Because of the ability to apply stresses at rates of loading in excess of the capabilities of currently used dynamic soil testing apparatus, the adaption of the SHPB technique to measure the dynamic response of soil seems a natural extension. The driving force for obtaining soil response at higher stress and strain-rate regimes has been the need to develop methods for estimating structural damage to military systems in or on soil. However, information on high strain-rate deformation of soils is also potentially useful in areas such as mining, overburden removal, earthquake engineering,, containment of ground nuclear tests and the study of impact and explosive cratering phenomena.

In the past three years, we have conducted over 200 experiments on soil specimens with a SHPB apparatus at the Los Alamos National Laboratory. These experiments have provided a considerable challenge and a substantial learning process. The use of soil as specimens in a SHPB experiment is not a trivial matter because soils have very low wave speeds ($\approx$ 300 m/s) in comparison to the traditional materials tested in the SHPB (e.g., steel, 5,000 m/s). Soils also exhibit nonlinear hysteretic behavior which will cause a stress wave to attenuate as it propagates through the soil (Hendron and Auld, 1968). In addition, the relatively low unconfined compressive strength of soil (e.g., $\leq$ 0.1 MPa) creates difficulties in controlling boundary conditions. The objective of this paper is to share with the community some of the peculiarities of using soil as a specimen material in a SHPB experiment and the techniques we have used to overcome the difficulties. We also present and discuss some of our early results.

THE SPLIT-HOPKINSON PRESSURE BAR

In 1914, Bertram Hopkinson devised a method to experimentally study the mechanical behavior of solids in response to short duration impulse loads. In this experiment Hopkinson used a long cylindrical steel bar to investigate the pressures produced by the detonation of gun cotton or the impact of a lead bullet. The pressures were estimated by measuring the momentum trapped in a time piece attached to the downstream end of the bar. For the experiments, Hopkinson assumed that the stress over the cross section of the bar was uniform (i.e., the stress state was one-dimensional) and the stress wave propagated down the bar without dispersion.

Davies (1948) conducted an extensive study that addressed these assumptions and the experimental method. He also improved the experimental method by designing a condenser unit to electrically measure the displacement of the pressure bar due to the applied stress wave. This allowed a precise stress-time curve to be constructed rather than the only approximate representation that could be obtained from Hopkinson's method. With the ability to measure surface displacements accurately, Davies was able to investigate Hopkinson's assumptions experimentally. Using the equation governing the longitudinal vibration of an infinitely long circular cylinder that was developed independently by Pochhammer (1876) and Chree (1889), Davies described the phenomenon of wave dispersion and established the accuracy of the experimental results to be about 3 percent, provided that $R/\lambda \leq 0.1$, where R is the radius of the pressure bar and λ is the wavelength of an individual frequency component of the applied stress wave.

With the experimental and theoretical foundations of the method established, Kolsky (1949) modified the apparatus to permit dynamic material properties to be determined by indirect measurements. By placing a specimen between two pressure bars fitted with condenser microphones, Kolsky developed relationships whereby the average stress, strain, and strain-rate in the specimen could be computed. This experimental method is now known as the Kolsky method or the split-Hopkinson pressure bar method.

A diagram of the experimental apparatus used in this research is shown in Figure 1. The apparatus is the property of the Geophysics Group at Los Alamos National Laboratory. The main components of the system are the gas gun, the reaction frame, and the incident and transmitter bars (additional components are noted in Figure 1). The incident and transmitter bars are constructed of Vascomax 350 CVM maraging steel that has been heat treated to sustain a yield stress of approximately 2 GPa. Each pressure bar is 60.3 mm in diameter and 1.22 m in length. The bars ride in teflon bearings that allow unrestricted motion in the horizontal plane.

The applied stress wave is initiated by the impact of a striker bar (which is propelled by the gas gun) on the incident bar (see Figure 2). The striker bar is constructed of the same material and has a slightly larger diameter (i.e., 60.5 mm) than the pressure bars. The amplitude of the stress wave is proportional to the velocity at which the striker bar impacts the incident bar, while the duration is a function of its length. Multiple impacts by the striker bar on the incident bar are prevented by venting the driving gas at the end of the launch tube.

The applied stress wave in the bars is monitored by resistance strain gauges mounted on the radial surface of the pressure bars. The strain gauges are mounted in pairs on opposite sides of the respective pressure bars and connected in a half-bridge configuration to nullify bending strains. The data recorded from the strain gauge bridges are filtered and preamplified and then routed to a data acquisition system. The data are read by a microcomputer and stored on a flexible disk for later processing on a larger machine.

The limitations of the SHPB experimental method are dependent on how well the assumptions required to reduce the data are satisfied. These assumptions are:

(1) there is a uniform distribution of axial and radial stress over the length of the specimen,

(2) the wave in the pressure bars propagates without dispersion,

(3) the stress state over the cross sectional area of the pressure bar is one-dimensional, and

(4) the interfaces between the pressure bars and the specimen are frictionless.

These are the basic assumptions made by Kolsky (1949). Felice (1985) has

established that these assumptions can be satisfied and/or corrected for when using soil specimens.

THEORY OF MEASUREMENT

Assuming that a one-dimensional stress state exists during the propagation of the applied stress wave, the particle velocity of the wave is given as

$$v = \frac{\sigma}{\rho C_o} \qquad (1)$$

where σ is the magnitude of the incident stress wave, ρ is the mass density of the bar, and C_o is the rod wave speed in the bar. The product ρC_o is commonly referred to as the characteristic impedance. A diagram of the SHPB near the specimen is shown in Figure 3.

If the characteristic impedance or area of the specimen is less than that of the pressure bars, when the applied compressive stress wave reaches interface 1, a portion of it will be reflected as a tensile wave and that portion of the stress wave which the specimen is able to support is transmitted through the specimen. When the portion of the stress wave propagating through the specimen reaches interface 2, the wave is once again partitioned, with a portion being reflected back into the specimen and a portion being transmitted into the transmitter bar. The reflected wave at interface 2 is compressive; hence, it will continue to traverse the specimen, increasing in amplitude with each transit. The result is that the net particle velocity of interface 1 is

$$v_1 = v_i - (-v_r) \qquad (2)$$

or

$$v_1 = \frac{\sigma_i - (-\sigma_r)}{\rho C_o} \qquad (3)$$

and the net particle velocity of interface 2 is

$$v_2 = \frac{\sigma_i - (-\sigma_r)}{\rho C_o} = v_t \qquad (4)$$

By taking the difference of the interface particle velocities, the rate at which the specimen is strained can be computed as

$$\dot{\varepsilon} = \frac{v_i - (-v_r) - v_t}{l} \qquad (5)$$

where l is the initial length of the specimen. The strain experienced by the specimen at any time t, can be computed by taking the integral of the strain-rate. The stress at each interface can be computed in a similiar fashion such that

$$\sigma_1 = \frac{(\sigma_i + (-\sigma_r))\, A_1}{A_2} \qquad (6)$$

$$\sigma_2 = \frac{\sigma_t\, A_1}{A_2} \qquad (7)$$

and the average stress in the specimen will be

$$\sigma_{avg} = \frac{(\sigma_1 + \sigma_2)\, A_1}{2A_2}, \qquad (8)$$

where A_1 is the area of the pressure bar and A_2 is the area of the specimen. These equations constitute the standard procedure for computing the average specimen response from the SHPB experimental data.

The magnitude of the waves in the above expressions are recorded by the strain gauges that are located a distance from the specimen-bar interfaces. For the analysis, the waves are shifted in time to the respective specimen-bar interface, e.g., the transmitted wave is shifted back by $\Delta x/Co$, where Δx is the distance between the strain gauge and the interface. As the propagating wave is dispersive (Davies, 1948) a phase correction must be applied to the waves in addition to shifting them in time. Follansbee and Frantz (1983) have developed a numerical procedure to account for wave dispersion that can easily be incorporated into the standard SHPB data reduction procedure. This is accomplished be transforming the recorded stress wave to the frequency domain then introducing a variation of phase velocity with wavelength based on an approximation to the fundamental mode of vibration of the dispersion equation and then inverting back to a time domain.

With soil specimens, the conditions assumed for the reduction of data from the SHPB experiment may not be met. In particular, the wave speeds in dry soil at low stress levels may be very low, e.g., 200 to 250 m/s. By constraining the deformation to be nearly uniaxial strain, a Lagrangian analysis technique that was developed for shock wave experiments can be adopted. For this analysis the equations of motion of the soil are

written such that stress is expressed in terms of velocity or stress and the temporal and spatial derivatives of the same. Because the calculation of stress at the incident bar-specimen interface involves the subtraction of two large numbers it is more appropriate for analysis to use the interface particle velocity. This method was developed by Seaman (1974) specifically for the analysis of uniaxial strain waves which attenuate as they propagate.

The Lagrangian analysis assumes that the velocity gauge does not affect the flow of the stress wave through the soil. This assumption is correct for interface 1 because the bar merely imposes a time-dependent boundary condition on the wave propagating into the soil. However, this assumption is certainly incorrect for interface 2 where the wave impinges on an almost rigid bar. Fortunately, the free-field Lagrangian velocity (i.e., that which would be observed by a massless transducer at the interface if the transmitter bar were composed of the same material as the specimen) can be estimated from the reflection properties at the interface.

Consider the experiment in pressure-particle velocity space as illustrated in Figure 4. If the impedance of the wave reflected back into the specimen at the transmitted interface is equal to that of the wave incident on the interface (n = 1 in Figure 4), the ratio of the free-field Lagrangian particle velocity, u_L, to the measured particle velocity, u_m, can be computed from the geometric relations

$$\frac{u_L}{u_m} = \frac{\rho_b D_b}{2\rho_s D_s} + \frac{1}{2} \qquad (9)$$

where ρ is the density and D is the wave speed, the subscripts b and s refer to the bar and soil, respectively. As a check, the pressures are related by

$$\frac{P_L}{P_m} = \frac{\rho_s D_s}{2\rho_b D_b} + \frac{1}{2} \qquad (10)$$

If the impedance of the reflected wave is n times that of the incident wave, the ratios are

$$\frac{u_L}{u_m} = \frac{\rho_b D_b}{(n+1)\rho_s D_s} + \frac{n}{n+1} \qquad (11)$$

$$\frac{P_L}{P_m} = \frac{n\rho_s D_s}{(n+1)\rho_b D_b} + \frac{1}{n+1} \qquad (12)$$

The velocity of the loading wave at the transmitter bar interface and that of the reflected wave can be obtained directly from experimental data. Occassionally, the second arrival at the transmitter bar specimen interface can be detected.

As long as the deformation of the soil specimen is smooth and the waves are compressive, the Lagrangian analysis technique can be applied. However, if the deformation of the specimen is not smooth, the reflection coefficient will not be constant and the free-field Lagrangian waveforms cannot be inferred. This would be the case if a specimen had a sharply defined yield point or if all the air voids in the specimen were closed. As the yield point is exceeded the reflection coefficient would decrease dramatically. At the point of zero air voids the reflection coefficient would increase. Also if the incident wave has a rarefaction phase this would likely have a substantialy higher impedance than the compression which would occur upon its reflection from the transmitter bar. The result would be a very complicated geometric configuration in the pressure-particle velocity plane.

SOIL SPECIMENS

The soils used in this research were sampled from two locations: the CARES-Dry site, located on the Luke Air Force Base, near Yuma, Arizona, and the McCormick Ranch test site located on Kirtland Air Force Base, New Mexico. The initial specimen parameters and a particle size distribution for these soils are shown in Table 1 and Figure 5, respectively. The compaction moisture and density combinations for specimens prepared from the McCormick Ranch soil ranged from dry of optimum to wet of optimum conditions as determined by the Harvard miniature compaction procedure i.e., a moisture content of 13.3 percent and a dry density of 1.87 gm/cc. The majority of experiments were performed with specimens prepared at or near optimum conditions. In most cases, a minimum of two experiments were conducted at each combination of specimen moisture content and density. The length of the specimens were either 12.7 mm or 6.35 mm. The specimens prepared from the Yuma soil all had moisture contents of 3.5 percent and wet densities of 1.77 gm/cc. the specimen lengths were 13 mm and 25 mm.

To achieve a nearly uniaxial strain environment for the experiments, the soil specimen was prepared by static compaction in a thick-walled confining cylinder. The material for the confining cylinder was either bearing bronze or steel with an axial hole slightly larger than the diameter of the pressure bars (see Figure 6). The confining cylinder served two purposes; first, to contain the soil specimen itself, and second, to confine the specimen to a state of nearly uniaxial strain, avoiding the effects of radial inertia. The confinement also prevented specimen distortion or barrelling during the experiment. This prevented friction forces from influencing the experimental results. As the ends confining the cylinder overlapped the pressure bars, tests were carried out to determine if the cylinder was transferring any stress to the transmitter bar. The results showed that the confining cylinder carried less than 0.1 percent of the applied stress during the dynamic loading.

To verify that a nearly uniaxial strain state was being achieved, calculations were performed comparing the radial strain experienced by the confining cylinder and the maximum longitudinal strain of the specimen. The radial strain was estimated by computing the radial deflection of the confining cylinder using thick-walled cylinder theory assuming the internal pressure was the maximum average stress sustained by the specimen. The computed radial strain of the confining cylinder for all experiments did not exceed one percent. For the dry specimens the radial strain was less than 0.1 percent of the longitudinal strain, and for the wet specimens the radial strain was less than six percent of the longitudinal. Hence, the specimens were constrained to a state of nearly uniaxial strain during the experiment.

EXPERIMENTAL RESULTS

Figure 7 shows the stress-strain response for a 12.7 mm specimen of McCormick Ranch soil to an applied stress of 400 MPa. The response is representative for the specimen lengths and applied stresses used in this research.

The stress-strain curve can be divided into three regions which describe the overall specimen response (see Figure 7). The first region, O to A, is where inertia effects act to oppose the equilibration of stress. The extent of this region can be estimated by the criterion of Davies and Hunter (1963) as well as experimentally (Felice, 1985). At A the specimen is considered to be in quasi-equilibrium and the deformation nearly homogeneous. Since the standard data reduction technique assumes that stress equilibration in the specimen is achieved, the results in this region are not to be considered reliable. To obtain data in this region a wave propagation analysis is required; hence the justification for introducing the Lagrangian analysis technique.

Region A to B is characterized by particle rearrangement into a denser packing and closing of the air voids. The strain at B is approximately equal to the initial gas porosity of the specimen (i.e., the volume of gas contained in the specimen divided by the total volume of the specimen). Hence, at B the specimen is in a nearly saturated condition. At this point the compressive resistance of the water becomes appreciable and the specimen will become strongly resistant to additional deformation (i.e., in region B to C).

An objective of this research was to show that the experimental results obtained with the SHPB technique could be replicated. Figure 8 shows the results of replicate experiments conducted at the nominal applied stress of 250 MPa and a specimen length of 6.35 mm. The applied stress is given in parentheses next to the experiment identification number. These results show that experimental replication can be achieved as the slopes of the stress-strain curves, the peak stress, and the strain at peak stress are directly comparable.

Figures 9 and 10 show the typical stress-strain response for the nominal specimen lengths of 6.35 mm and 12.7 mm, respectively, to a range of applied stresses. It can be observed that the average stress experienced by the specimen increased with increasing applied stress independent of the specimen length. For both specimen lengths, the stress-strain response is very similar for applied stress up to 400 MPa, with some increase in stiffness observed at the higher stresses. For all applied stress levels, the specimens began to stiffen at strains approximately equal to the initial gas porosity. For both specimen lengths and at all applied stresses, the strain at peak stress experienced by the specimen exceeded the initial gas porosity of the specimen.

Figure 11 compares the stress-strain response of specimens to the same applied stress but with different specimen lengths. It is observed that the strain experienced by the shorter specimen exceeded that of the longer specimen. Also the longer specimen showed greater stiffness at a lower strain than the shorter specimen. This apparent discrepancy in response between the two specimen lengths results from greater initial gas porosity of the shorter specimen.

To observe how moisture content variations affect stress-strain response, specimens were prepared at the nominal moisture contents of 7, 13, and 15 percent. The experimental results are shown in Figures 12 and 13. These figures show that the average stress experienced by the specimen increased while the strain at peak stress decreased with increasing moisture content. As with the other stress-strain curves shown, there is a marked break in slope near a strain equal to the initial gas porosity. This change in slope is not observed for the 12.7 mm specimen with the lowest moisture content (experiment 135); however, the maximum strain (approximately 16 percent) did not approach the initial gas filled porosity of 23.4 percent.

Figure 14 illustrates the application of the Lagrangian analysis technique to SHPB data. The variation in the amplitudes of the incident waves did not exceed $\pm$ 2 percent. Two experiments were conducted with a nominal specimen length of 25 mm and two with nominal specimen lengths of approximately 13 mm. The data from experiments 21, 23, and 24 show that the reflections from the transmitter bar interface travel at about 1.6 times faster (i.e., Lagrangian wave speed) than the incident wave through the specimen. Hence, the reflection coefficient is 1.6. To perform the analysis, the incident bar interface velocity was established as the first gauge, the transmitter bar specimen interface velocity of the 13 mm specimen as the second gauge, and the transmitter bar specimen interface velocity of the 25 mm specimen as the third gauge position. The results of the Lagrangian analysis for the experiments conducted on the Yuma soil are shown in Figures 15 and 16.

DISCUSSION

In one-dimensional compression the general stress-strain response exhibited by soil is S-shaped. For small stress changes, yielding is observed with the stress-strain curve concave to the strain axis. For large stress changes, the behavior is characterized by stiffening with the stress-strain response reversing curvature (i.e., concave to the stress axis). The general specimen stress-strain response observed in this research is consistent with the above description and similar to that found by other investigators who performed experiments on similar soils, but at lower rates of loading (e.g., Jackson, 1968; Calhoun and Kraft, 1966).

In nearly all the experiments conducted, the strain at peak stress was greater than the initial gas porosity of the specimen. In one-dimensional confined compression it is anticipated that as a soil specimen strains the pore air will be compressed until the specimen becomes saturated, at which time the compressive resistance of the pore water will approach that of the soil skeleton. Therefore peak strains greatly in excess of the initial gas porosity of the specimen are unlikely. However, we have observed peak strains as great as a factor of two greater than the specimen initial gas porosity. There are several factors which have been identified that can account for this discrepancy: (1) loss of soil and moisture, (2) compression of the pore water, and (3) radial expansion of the confining cylinder. The strain contribution for each of these factors has been analyzed and incorporated into a strain correction that has been used to account for the observed discrepancy (Felice, 1985).

At strains less than the initial gas porosity the compressibility of the specimens is nearly constant (see Figures 9 and 10 and Table 1). At strains in excess of the initial gas porosity, the compressibility of the specimens is again nearly constant, but with a value greater than the initial compressibility. For example, in Figure 10 the tangent modulus for experiment 134 at four percent strain is 0.2 GPa whereas at 11 percent it is 1.5 GPa, which is approximately that of water (2 GPa). As the soil strains approach the initial gas porosity and exceed it, the response changes from being governed by the soil mass to being controlled by the pore water. A similar response has been observed for McCormick Ranch soil subjected to high hydrostatic compression (Mazanti and Holland, 1970). The observation that the initial gas porosity of the specimen is a governing parameter in

soil response is consistent in all the experiments conducted.

To determine the strain-rate sensitivity, stress-strain-rate curves at constant strains were constructed for each nominal specimen length. The data were taken from experiments conducted at the nominal applied stresses of 250 and 400 MPa. The results are presented in Figures 17 and 18 for the 6.35 mm and the 12.7 mm long specimens compacted at moisture and density combinations near optimum, respectively. The dashed lines are the average stress-strain-rate trajectories for a given applied stress. The solid lines connect points of constant strain between the stress-strain-rate trajectories.

The degree to which the material is strain-rate dependent can be determined directly from the slope of the constant strain curves connecting the stress-strain-rate trajectories. If the slope is zero, it can be concluded that the material response is independent of strain-rate. In Figures 17 and 18 the stress which produced a given strain did not increase with increased strain-rate at strains less than the initial gas porosity of the specimen. This indicates that material response is not dependent on strain-rate for strains less than the initial gas-filled porosity. Figure 19 compares the stress-strain path for the SHPB experiments with quasi-static uniaxial strain tests for the Yuma soil. These curves are virtually indistinguishable, supporting the conclusion that for strain-rates up to 5,000 s^{-1} and strains less than the initial gas porosity of the specimen, material response is independent of strain-rate. From Figure 15 the strain-rates computed using the Lagrangian analysis are 1,800 to 5,000 s^{-1}, about twice as great as those determined from the standard analysis. This is because the deformation is not distributed uniformly through the specimen during the wave propagation portion of the experiment (which is represented by the initial loading).

The loading behavior of the Yuma soil has been represented by a one-dimensional model that treats the soil as a collection of cells (Gaffney, 1985). A typical cell consists of two rigid half cubes of a sand grain, ℓ on a side, separated by a void and a pillar of a Bingham material of dimension

$$\frac{\ell \times \ell \times \ell\phi_c}{1-\phi_s} \qquad (13)$$

where ϕ_c and ϕ_s are the volume fractions of clay and sand, respectively. Considering the strength, "viscous" flow, and horizontal and vertical inertia of the deforming clay pillar, along with the inertia of the sand, the stress-strain relation for the cell can be written as

$$\sigma = \pm \frac{2\phi_c\sigma_o}{1-\phi_s-\varepsilon} + \frac{3\mu\phi_c^3\phi_s^2\dot{\varepsilon}}{4(1-\phi_s-\varepsilon)^6} + \frac{\rho_c\phi_c^3\ell^2\dot{\varepsilon}^2}{2(1-\phi_s-\varepsilon)^5} + \ell^2\left[\frac{\rho_c\phi_c^3}{4(1-\phi_s-\varepsilon)^4} + \frac{\rho_s}{\phi_s} + \frac{\rho_c\phi_c}{\phi_s^2}\right]\ddot{\varepsilon} \qquad (14)$$

where ρ_s and ρ_c are the densities of the sand and clay, respectively, and σ_o is the strength and μ the "viscosity" of the Bingham material.

Although the formulation involves seven parameters (σ_o, μ, ϕ_s, ϕ_c, ρ_c, ρ_s, ℓ), only σ_o and μ cannot be determined from standard laboratory test data. The value of ρ_s is the grain density of the sand. The value of ρ_c can be calculated from the grain density of the silt and clay fraction plus the water content. Values for ℓ, ϕ_c, and ϕ_s can be obtained from a particle size analysis. For the Yuma soil, ϕ_s and ϕ_c are 0.57 and 0.15, respectively, and the mean size of the sand fraction is 0.5 mm. The sand is predominantly quartz and feldspar, hence ρ_s was taken as 2,650 kg/m^3. We estimated ρ_c to be 2,400 kg/m^3.

The low strain portion of the static behavior is most sensitive to the distribution of ϕ_c and σ_o. A beta-distribution for ϕ_c has been assumed

$$P(\phi_c) = B(1.5, 2.25)\left(\frac{\phi_c}{1-\phi_s}\right)^{0.5}\left(1-\frac{\phi_c}{1-\phi_s}\right)^{1.25} \qquad (15)$$

where B is the beta function. With a yield stress of 10 MPa we get a static stress-strain curve as shown in Figure 20. With $\mu = 10^3$ Pa · s, the model fits both the SHPB and quasi-static data very well.

In simulating the behavior of the Yuma soil, σ_o and μ have been selected to fit the data. There is an extensive amount of literature on the rheology of clay-water mixtures. For most mixtures, the strength and "viscosity" used here would be high, but these properties are sensitive to the solids: water ratio at high solids

concentration (Norton, Johnson, and Lawrence, 1944). No data have been located for mixtures as dry as ours. However, extrapolation from four times our water contents yields values on the order of those used.

The soil model requires further development before it can be considered to be predictive. Nevertheless, it does permit some evaluation of the relative importance of inertial effects and direct strain-rate effects in soil.

CONCLUSION

This paper presents the results of an experimental program conducted with soil specimens subjected to high stresses and strain-rates using the split-Hopkinson pressure bar apparatus. Experimental results, presented in terms of stress-strain response, show the ability to achieve experimental replication and soil response to a range of applied stresses and strain-rates at different compaction conditions. The results presented show that the material is strain-rate insensitive at strains less than the initial gas porosity of the specimen. A micromechanical model has been devised to assist in the understanding of the soil response.

We have demonstrated that the split-Hopkinson pressure bar technique is a tool that can be used to examine the dynamic response of soil in regimes beyond the capabilities of current devices. This will assist in the understanding of soil behavior in that environments can now be provided in the laboratory that more closely reflect those in the field. Hence, the need to extrapolate laboratory data is reduced. This will lead to a decrease in the time required to evaluate the adequacy of a model to a particular problem as well as better models because the material properties can be evaluated from data that more closely duplicate field conditions.

REFERENCES

1. Calhoun, D.E. and Kraft, D.C., 1966. An Investigation of the Dynamic Behavior of a Partially Saturated Silt with Applications to Shock-Wave Propagation, AFWL-TR-65-176, Air Force Weapons Laboratory, Kirtland AFB, New Mexico.

2. Chree, C., 1889. "The Equations of an Isotropic Elastic Solid in Polar and Cylindrical Coordinates, their Solutions and Applications," Transactions of the Cambridge Philosophical Society, Vol. 14, pp. 250-369.

3. Christensen, R.J., Swanson, S R., and Brown, W.S., 1972. "Split-Hopkinson-bar Tests on Rocks under Confining Pressure," Experimental Mechanics, Vol. 12, No. 11, pp. 508-513.

4. Davies, E.D. and Hunter, S.C., 1963. "The Dynamic Compression Testing of Solids by the Method of the Split Hopkinson Pressure Bar," Journal of the Mechanics and Physics of Solids, Vol. 11, pp. 155-179.

5. Davies, R.M., 1948. "A Critical Study of the Hopkinson Pressure Bar," Philosophical Transactions of the Royal Society of London, Series A, Vol. 240, pp. 375-457.

6. Felice, C.W., 1985. "The Response of Soil to Impulse Loads Using the Split-Hopkinson Pressure Bar Technique," Dissertation presented to the University of Utah, in partial fulfillment of the requirements for the degree of Doctor of Philosophy.

7. Follansbee, P.S. and Frantz, C.E., 1983. "Wave Propagation in the Split Hopkinson Pressure Bar," Journal of Engineering Materials and Technology, Vol. 105, pp. 61-66.

8. Gaffney, E.S., 1985. Preliminary Constitutive Model for Alluvium, Office Memo ESS-5:85-00-410, Los Alamos National Laboratory, Los Alamos, New Mexico.

9. Gaffney, E.S. and Brown, J.A., 1984. Dynamic Material Properties for Dry CARES Alluvium, LA-UR-84-3795, Los Alamos National Laboratory, Los Alamos, New Mexico.

10. Hendron, A.J. and Auld, H.E., 1968. "The Effect of Soil Properties on the Attenuation of Airblast-Induced Ground Motion," in Proceedings of the International Symposium on Wave Propagation and Dynamic Properties of Earth Materials, University of New Mexico Press, Albuquerque, New Mexico, pp. 29-47.

11. Hodge, K.G. and Wasley, R.J., 1969. "Dynamic Compressive Behavior of Various Foam Materials," in High Speed Testing. Vol. 6, Interscience, New York, pp. 97-109.

12. Hopkinson, B., 1914. "A Method of Measuring the Pressure Produced in the Detonation of High Explosives or by the Impact of Bullets," Philosophical Transactions of the Royal Society of London, Series A. Vol 213, pp. 437-456.

13. Jackson, J.G. Jr., 1968. Factors that Influence the Development of Constitutive Relations. Misc. Paper No. 4-980, U.S. Army Engineer Waterways Experiment Station, Vicksburg, Mississippi.

14. Kolsky, H., 1949. "An Investigation of the Mechanical Properties of Materials at Very High Rates of Loading," Proceedings of the Physical Society, Section B, Vol. 62, pp. 676-700.

15. Lindholm, U.S., 1964. "Some Experiments with the Split Hopkinson Pressure Bar," Journal of the Mechanics and Physics of Solids, Vol. 12, pp. 317-335.

16. Mazanti, B.B. and Holland, C.N., 1970. Study of Soil Behavior Under High Pressure. Contract Report S-70-2, U.S. Army Engineer Waterways Experiment Station, Vicksburg, Mississippi.

17. Nagy, A. and Meulenhaupt, H.J., 1983. Description and Operating Manual for the 2.375 Inch Split Pressure Bar System for Dynamic Material Testing in Compression. Contract No. N68-6525G-1, Prepared for the In Situ Science Group, Los Alamos National Laboratory, Los Alamos, New Mexico, by the Department of Materials Sciences, Southwest Research Institute.

18. Norton, F.H., A.L. Johnson, and W.G. Lawrence, 1944. "Fundamental Study of Clay:VI, Flow Properties of Haolinite-Water Suspensions," Journal of Ceramics, Vol 27, pp. 149-169.

19. Pochhammer, L., 1876. "On the Propagation Velocities of Small Oscillations in an Unlimited Isotropic Circular Cylinder," Journal fur die Reine und Angewandte Mathematik, Vol 81, pp. 324-326.

20. Seaman, L., 1974. "Lagrangian Analysis for Multiple Stress or Velocity Gauges in Attenuating Waves," Journal of Applied Physics. Vol. 45, pp. 4303-4310.

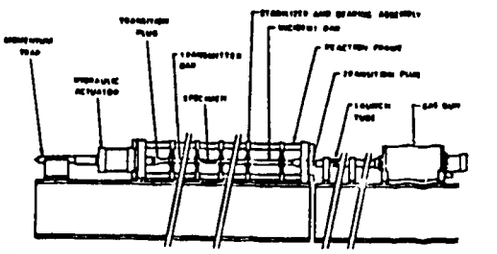

Figure 1. Split-Hopkinson pressure bar system arrangement (Nagy and Muelenhaupt, 1983)

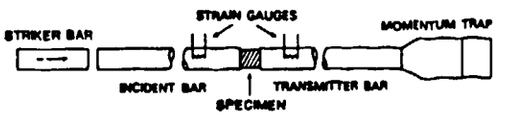

Figure 2. Split-Hopkinson pressure bar schematic.

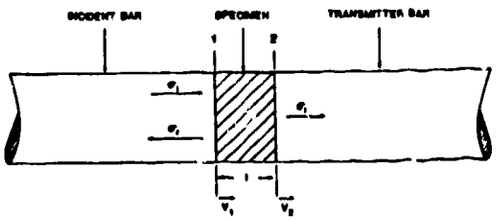

Figure 3. Specimen in place between pressure bars.

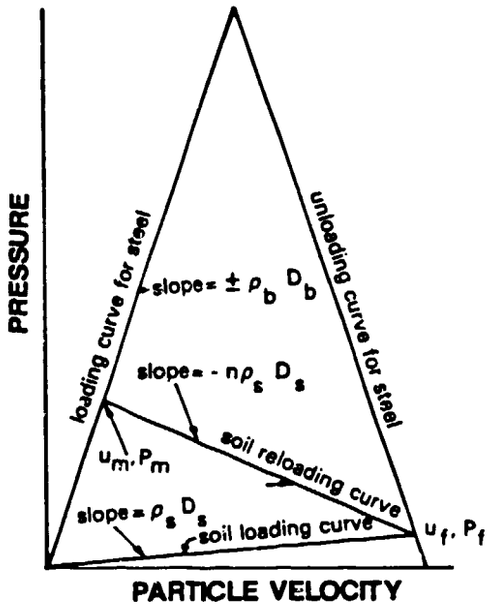

Figure 4. Pressure-particle velocity plot of split Hopkinson bar experiment showing relations used in converting transmitter bar data to free-field Lagrangian equivalent.

Table 1
Initial Specimen Parameters

Experiment No.	Specimen Length (cm)	Moisture Content (%)	Gas Porosity (%)	Wet Density (g/cc)	Void Ratio	Degree of Saturation (%)
21	1.27	3.5	30.0	1.77	0.46	17.0
22	2.54	3.5	30.0	1.77	0.46	17.0
23	1.27	3.5	30.0	1.77	0.46	17.0
24	2.54	3.5	30.0	1.77	0.56	17.0
115	0.635	11.8	10.6	2.04	0.46	46.8
116	0.637	11.2	8.1	2.10	0.41	72.8
117	0.635	10.7	8.5	2.10	0.41	70.5
118	0.645	10.6	10.3	2.07	0.44	65.9
119	0.645	10.8	9.9	2.08	0.42	64.8
132	1.269	12.5	6.9	2.10	0.43	77.2
134	1.258	12.8	5.8	2.12	0.41	80.2
135	1.107	7.0	23.8	1.84	0.55	38.1
136	1.223	15.1	5.2	2.06	0.48	84.1
139	0.609	7.0	17.7	1.98	0.44	42.3
145	1.265	11.8	6.2	2.13	0.40	78.3
163	0.631	12.9	8.8	2.13	0.41	83.8
164	1.298	12.9	7.5	2.07	0.45	76.0
167	0.622	18.0	8.2	2.12	0.43	86.3

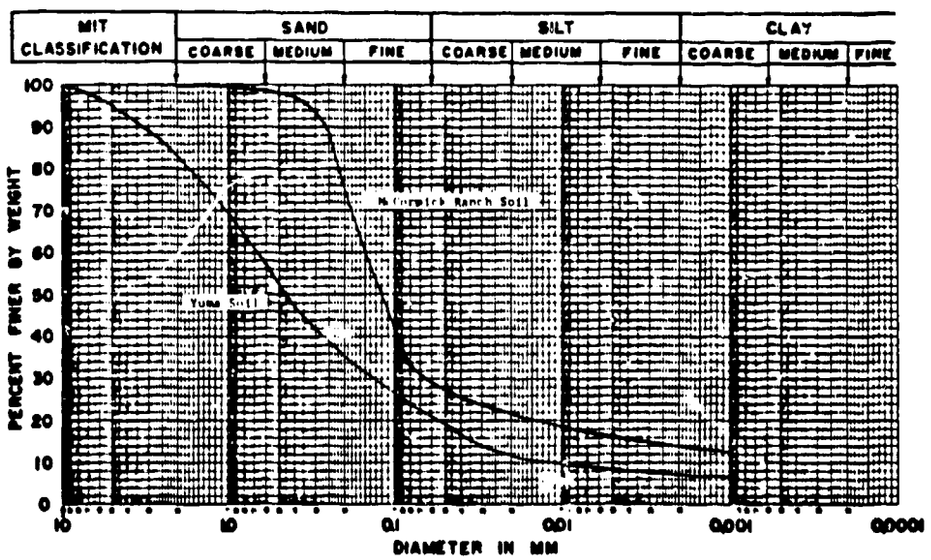

Figure 5. Particle size distributions

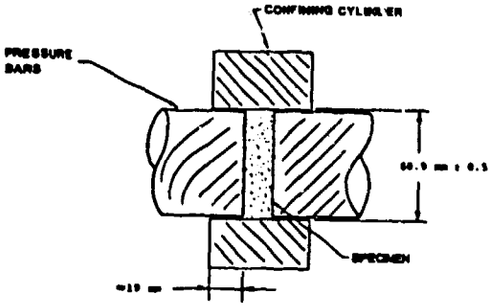

Figure 6. Confining cylinder with specimen positioned between the pressure bars.

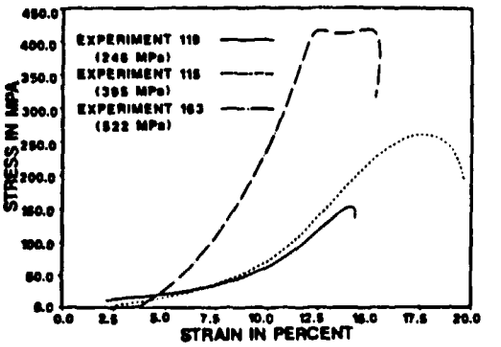

Figure 9. Stress-strain response for 6.35 mm specimens to a range of applied stresses.

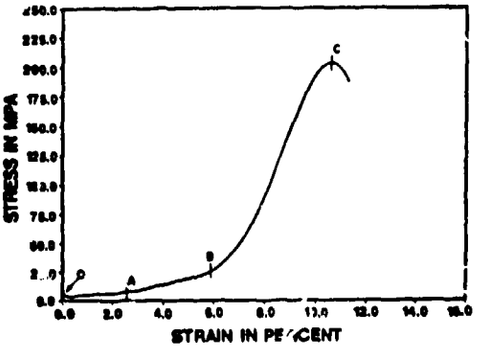

Figure 7. Stress-strain response for experiment 132.

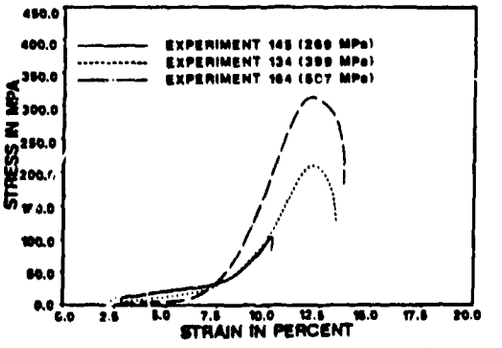

Figure 10. Stress-strain response for 12.7 mm specimens to a range of applied stresses.

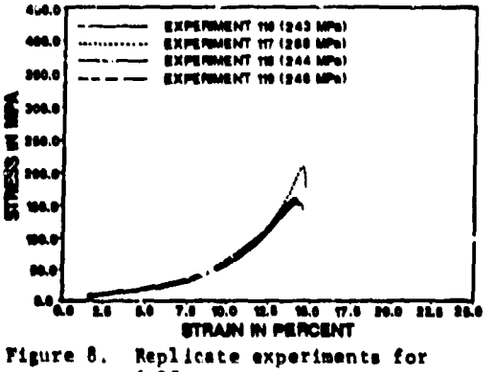

Figure 8. Replicate experiments for 6.35 mm specimens at an applied stress of approximately 250 MPa.

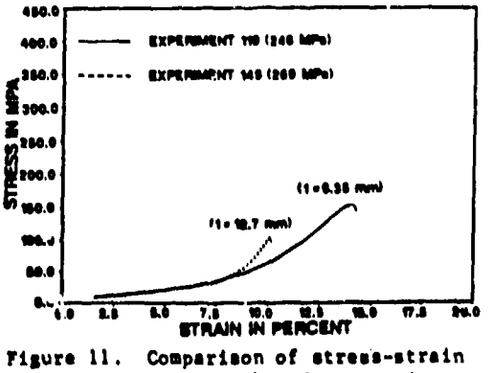

Figure 11. Comparison of stress-strain response based on specimen length to an applied stress of approximately 250 MPa.

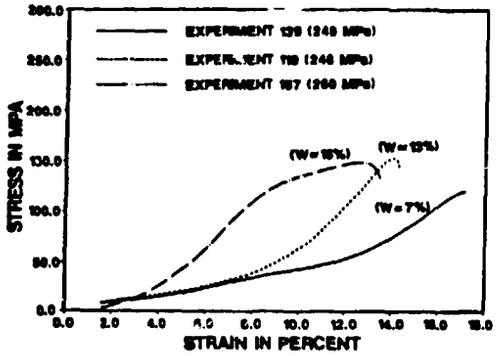

Figure 12. Comparison of stress-strain response for 6.35 mm specimens based on moisture content (w) to an applied stress of approximately 250 MPa.

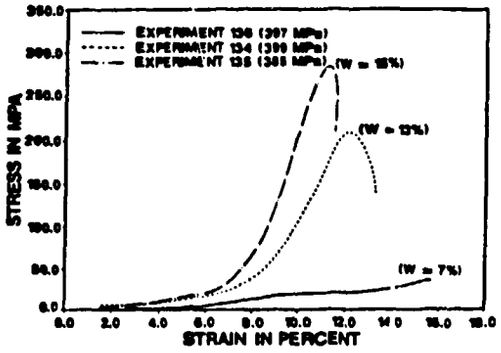

Figure 13. Comparison of stress-strain response for 12.7 mm specimens based on moisture content (w) to an applied stress of approximately 400 MPa.

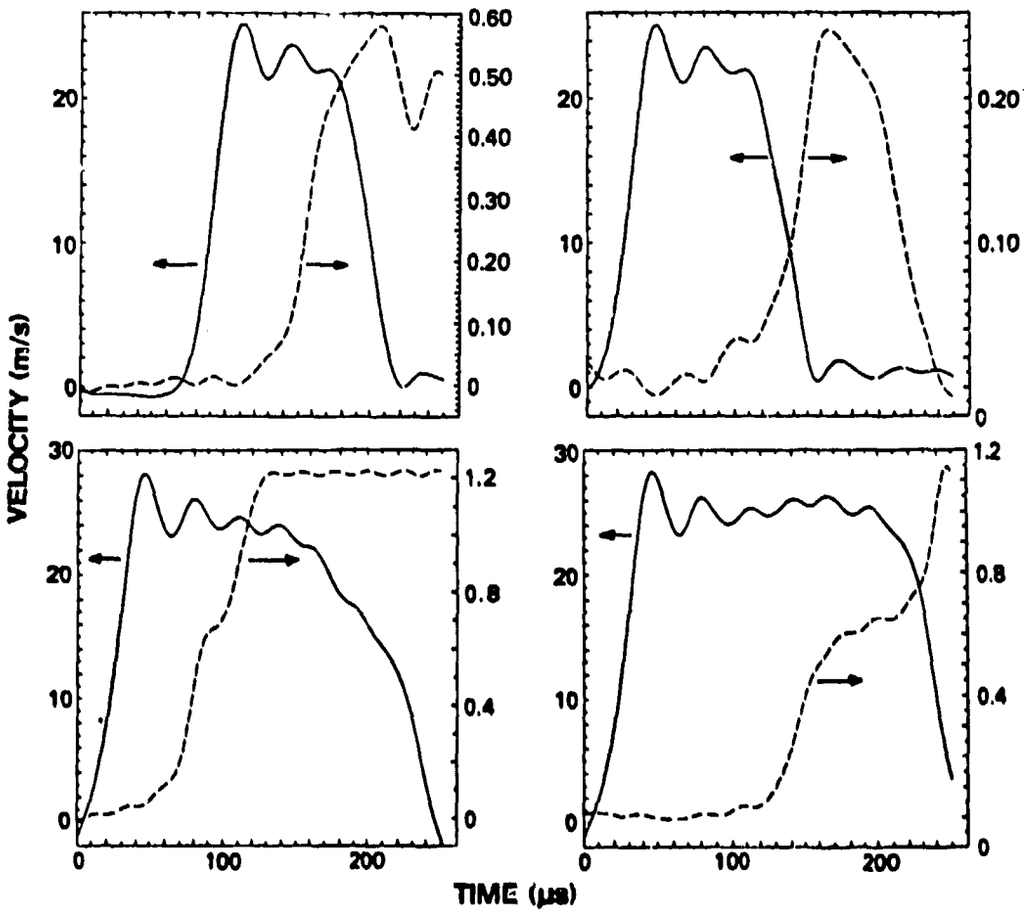

Figure 14. Interface velocity histories for four Hopkinson bar tests of dry desert alluvium.

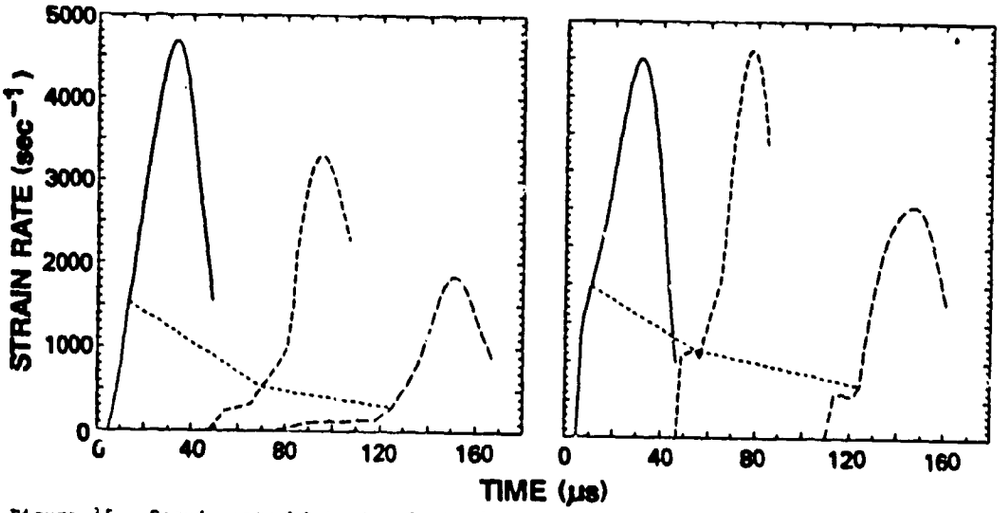

Figure 15. Strain-rate histories derived from data in Figure 14.

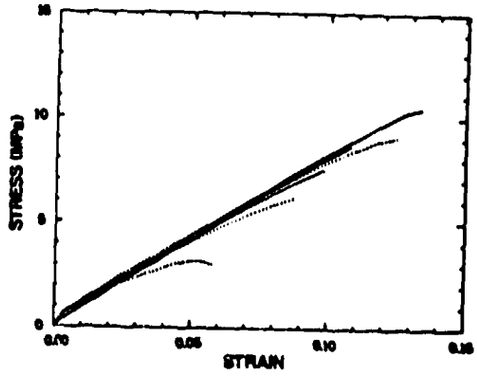

Figure 16. Stress-strain paths derived for initial loading of desert alluvium in Hopkinson bar.

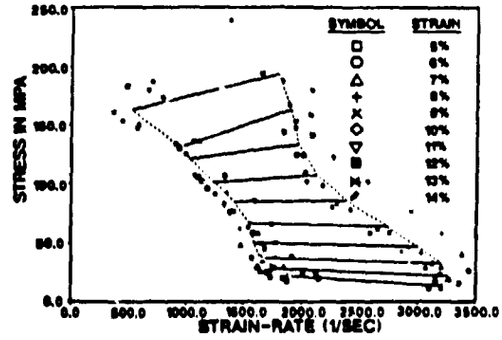

Figure 17. Stress-strain-rate plot for 6.35 mm specimens compacted at optimum conditions.

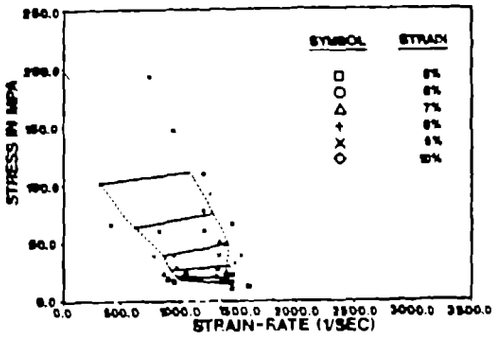

Figure 18. Stress-strain-rate plot for 12.7 mm specimens compacted at optimum conditions.

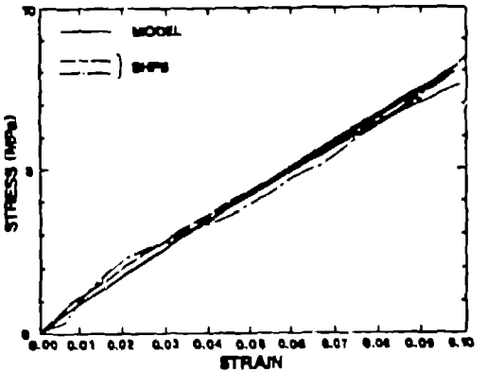

Figure 20. Stress-strain paths in dry alluvium

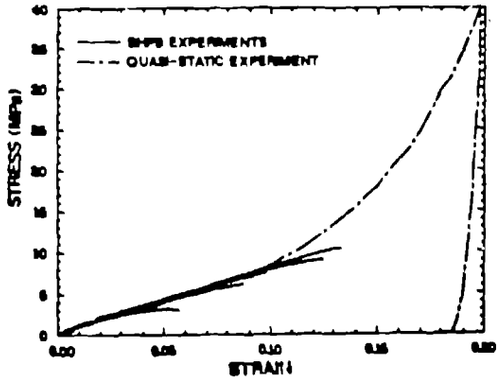

Figure 19. Stress-strain paths for several types of uniaxial strain deformation of dry CARES alluvium: solid = Hopkinson bar, chain dash = quasistatic.

DISCLAIMER